ELSEVIER

J. Non-Newtonian Fluid Mech. 147 (2007) 11–22

Journal of Non-Newtonian Fluid Mechanics

www.elsevier.com/locate/jnnfm

The atomization of viscoelastic fluids in flat-fan and hollow-cone spray nozzles

Jeffery C. Thompson, Jonathan P. Rothstein *

Department of Mechanical and Industrial Engineering, University of Massachusetts, Amherst, MA, USA

Received 5 July 2006; received in revised form 13 June 2007; accepted 16 June 2007

Abstract

This article reports experimental observations of the flow kinematics and stability of thin fluid sheets produced by a series of commercially available flat-fan and hollow-cone spray nozzles for a series of viscoelastic wormlike micelle solutions. As the flow rate through the nozzle is increased, the sheets of viscoelastic fluid grow larger and eventually becoming unstable and atomizing into drops. For the sheets of water produced by the flat-fan nozzles, the fluid rims of the sheets were found to destabilize first. The addition of viscoelasticity was found to stabilize the rim while simultaneously destabilizing the internal fluid sheet. What results is a series of novel flow structures comprised of highly interconnected filaments created by the growth of multiple internal holes that develop within the fluid sheet. Increasing viscoelasticity of the test fluid was found to stabilize the thin films produced by both the flat-fan and hollow-cone spray nozzles, thereby shifting the break-up of the sheets to larger flow rates. However, beyond the critical flow rate for sheet rupture, increases to the fluid elasticity were found to alter the dynamics of the atomization of the viscoelastic fluid sheets by increasing the number and growth rate of holes in the sheet while simultaneously reducing the initiation time for sheet rupture.

Keywords: Atomization; Wormlike micelle solutions; Surfactant solutions; Viscoelastic

1. Introduction

In this article we report on the experimental observations of the flow kinematics and stability of thin fluid sheets produced by a series of commercially available flat-fan and hollow-cone spray nozzles for a series of viscoelastic wormlike micelle solutions. The structure, kinematics and stability of thin films have been well studied both experimentally and analytically throughout the literature for Newtonian fluids [1–4]. However, despite the importance of these fluids and flows to a host of commercial and industrial applications such as agrochemical spraying, spray coating, and inkjet printing, little work has been done to study the break-up of thin films of viscoelastic fluids [5–10]. The studies that do exist focus primarily on correlating atomization characteristics and droplet size distribution measurements to changes in polymer concentration, molecular weight and fluid rheology. These correlations are often valid only for a specific nozzle design. The mechanisms of break-up in these systems are still not well understood.

A good deal of literature does, however, exist describing the role of viscoelasticity on forestalling the break-up of laminar capillary jets [11]. The break-up dynamics of liquid jets are governed by the extensional viscosity, η_E, and the surface tension, σ, of the fluid. For polymeric or wormlike micelle solutions, the shear and extensional viscosities can be strong functions of the flow kinematics, the rate of deformation and the deformation history, $\eta = f(\dot{\gamma}, \gamma, t)$. The dynamical response of the fluids in extensional flows is quite different than in simple shear. Whereas the shear viscosity will often heavily thin with increasing shear rate, the extensional viscosity can increase by several orders of magnitude with increasing strain [12]. This strain hardening has been shown to stabilize viscoelastic jets while retarding satellite drop formation and increasing the main droplet size [11,13,14].

As the length of the fluid jet exceeds the circumference, they become unstable against break-up into droplets [13,15]. In the small Ohnesorge number regime, $\mathrm{Oh} = \eta/\sqrt{\rho\sigma R} << 1$, this break-up is resisted by inertia; the characteristic time for break-up of fluid jets is approximately the inertio-capillary or Rayleigh timescale, $\tau_R = (\rho R^3/\sigma)^{1/2} \approx 10^{-3}$ s. Here σ is the surface tension of the fluid jet, R the jet's radius, ρ the mass density of the fluid, and η is its shear viscosity. The viscoelasticity of the jet can forestall the break-up of laminar

* Corresponding author.
E-mail address: rothstein@ecs.umass.edu (J.P. Rothstein).

0377-0257/$ – see front matter © 2007 Elsevier B.V. All rights reserved.
doi:10.1016/j.jnnfm.2007.06.004

capillary jets [11]. For these fluids the Ohnesorge number is typically large $Oh \gg 1$, the break-up of the jet is resisted by the fluid viscosity, and the characteristic timescale for break-up is the visco-capillary timescale $\tau_v = \eta R/\sigma$. For a viscoelastic material, elasticity becomes important when the characteristic viscoelastic timescale, λ, approaches the characteristic timescale of the flow. In other words, when the Deborah number based on the extension rate, $\dot{\varepsilon}$, developed within the jet becomes greater than one, $De = \lambda\dot{\varepsilon} > 1$. For these viscoelastic fluids, it is the extensional viscosity η_E and not the shear viscosity that resists the break-up of the fluid jet. The characteristic time for jet break-up is given by the viscoelastic-capillary timescale $\tau_E = \eta_E R/\sigma$ [16]. For polymer and wormlike micelle solutions, the extensional viscosity can increase by several orders of magnitude as the extension rate and the accumulated strain are increased (the Trouton ratio can become quite large, $Tr \equiv \eta_E/\eta > 1000$) [12,17–19]. Consequently, strain hardening has been shown to delay the break-up of viscoelastic jets by dramatically increasing the viscoelastic-capillary timescale [11,14,20,21].

The stability and break-up of viscoelastic fluid sheets is not as well studied nor as well understood. Harrison et al. [8] investigated the effect of polymer concentration and rigidity on swirl-type hollow-cone spray nozzle. They demonstrated that independent of the polymer rigidity, very low concentrations of polymer increased the angle of the hollow cone produced by the nozzle and enhanced the break-up and atomization process. As the concentration was increased, the increased viscoelasticity and specifically increased extensional viscosity of the polymer solutions were found to reduce the cone-angle and negatively impact the atomization. Eventually, at a large enough concentration, the hollow cone could not be formed and a 'rope' was formed as the spray cone collapsed [8]. Xing et al. [5] investigated the atomization of water-born latex coatings. Their study and that of Mun et al. [6] demonstrated that stabilization of viscoelastic fluid sheets could be correlated directly to increases of extensional viscosity. Additionally, it has been demonstrated that increasing extensional viscosity increased the average size of the spray droplets and broadened the drop size distribution [5,6]. Mun et al. [6] also showed that it may be necessary to redesign the current commercially available nozzles if they are to be optimized for viscoelastic fluids.

Brenn et al. [10] performed a linear stability analysis on a non-Newtonian liquid sheet moving within an inviscid gas. They showed that unlike a liquid jet, for a liquid film surface tension is stabilizing and not destabilizing. The sheets are destabilized by aerodynamic effects. The fluid viscosity also stabilizes the sheets, but the elasticity of the non-Newtonian fluid strongly destabilizes the sheet increasing the growth rates of both symmetric and anti-symmetric two and three-dimensional disturbances [10]. What is interesting is that many of the results of Brenn et al.'s [10] linear stability analysis for this very idealized version of a thin viscoelastic sheet do not agree with the experimental observations of the atomization of non-Newtonian liquids using commercial spay nozzles [5,6,8] and impinging liquid jets [9] where the transition from stable to unstable flow was found to move to larger flow rates and Weber numbers with increasing elasticity number.

Experiments have shown that as the flow rate is increased, the fluid sheets produced by flow nozzles have been observed to transition through a series of different flow regimes. Aerodynamic forces are often the source of the initial disturbances in the fluid sheet. For low viscosity Newtonian fluids such as water these out-of-plane oscillations continue to grow with flow strength resulting in a flapping motion that eventually results in the atomization of the sheet [2]. In some cases the atomization of the sheet is initiated by a capillary-driven rim instability [22]. With more viscous Newtonian fluids, fingers can appear along the rim producing a flow structure that Bush and Hasha described as fluid 'fishbones' for the case of impinging fluid jets [9,22].

Miller et al. [9] studied the flow produced by impinging jets of viscoelastic fluids. They found that although oscillations were observed within the rim of the fluid sheet, the increased viscosity and the elasticity of the micelle solutions reduced their amplitude to the point that no fingering was observed. Above a critical flow rate, the sheets were found to destabilize through a randomly located internal failure producing a series of complicated interconnecting internal rims Miller et al. called 'fluid webs' and 'fluid tendrils' [9].

In the sections that follow, we will report on the experimental observations of the flow kinematics and stability of thin fluid sheets produced by a series of commercially available flat-fan and hollow-cone spray nozzles for a series of viscoelastic wormlike micelle solutions. In Section 2, we will describe the experimental procedure and the rheology of the test fluids. In Section 3, we will present our results and demonstrate the role of viscoelasticity on the atomization of thin films. Finally, in Section 4 we will conclude.

2. Experimental

2.1. Flow geometry and experimental setup

To generate the fluid sheets, fluid was pumped through a series of stainless steel flat-fan spray nozzles with expansion angles of $\beta = 30^\circ$, 65° and 120° and a hollow-cone spray nozzle with an expansion angle of $\beta = 70^\circ$ all purchased from McMaster Carr. These are commonly used commercial nozzles use for the atomization of liquids. Volume flow rates of up to $Q = 4 \times 10^{-6}$ m^3/s were achieved using one or more identical syringes driven by a linear stepper motor. Images and schematic diagrams of the nozzles used are provided in Fig. 1. Images of the thin films were taken with both a digital SLR camera (Nikon D70) with exposure times of 1/4000th of a second and a high-speed digital video camera (Phantom V4.2) capable of capturing video at 90,000 frames per second, but were primarily used between 1000 and 4000 frames per second.

2.2. Test fluids

A series of viscoelastic wormlike micelle solutions containing between 10 and 25 mM cetyltrimethylammonium bromide (CTAB) and equal molarities of sodium salicylate (NaSal) in distilled, deionized water were used in these experiments. Each

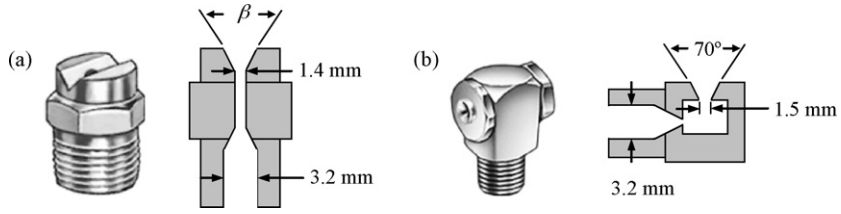

Fig. 1. Schematic diagram of the (a) flat-fan and (b) hollow-cone spray nozzles used in these experiments.

of these solutions is well above the critical micelle concentration, which for CTAB in pure water is CMC = 9×10^{-4} M [23]. At these concentrations, the wormlike micelle solutions are concentrated and entangled with significant number of entanglement points per chain [23]. The solutions were prepared and allowed to equilibrate at room temperature for several days before experiments were performed.

2.3. Shear rheology

The steady and dynamic shear rheology of the test fluid was characterized using a TA cone-and-plate controlled stress rheometer (Model AR2000) with a 6 cm diameter and 1° truncated cone. The micelle solutions were loaded and allowed to equilibrate at $T = 25\,^{\circ}$C for several minutes. The samples were not presheared. In the regime of linear deformation imposed by these small amplitude oscillatory shear flows, it has been shown that wormlike micelle solutions can be accurately modeled by a Maxwell model having just one or two relaxation times [24]. In Fig. 2, the storage modulus, G', and loss modulus, G'', of the wormlike micelle solutions with concentrations of 10, 17.5 and 25 mM CTAB and NaSal are plotted as a function of angular frequency, ω, along with the prediction of a single mode Maxwell model. In Table 1, the zero-shear-rate viscosity η_0 and relaxation time λ for each viscoelastic surfactant solution are listed. The linear viscoelastic data and the predictions of the single mode Maxwell models are in good agreement for all of the wormlike micelle solutions tested over much of the dynamic range. However, deviations are observed at large angular frequencies corresponding to the Rouse-like behavior of the micelle between entanglement points [25]. This deviation, which becomes more pronounced as the concentration of surfactant and salt and therefore the number of entanglements per chain are reduced, is consistent with observations in the literature and can be used to calculate the characteristic timescale for break-up and reformation of the micelles [26,27].

Table 1
Parameters characterizing the rheology of the CTAB and NaSal wormlike micelle solutions

CTAB (mM)	NaSal (mM)	η_0 (Pa s)	λ (s)	G (Pa)	El
10	10	5.0	18	0.28	4.3×10^4
17.5	17.5	41	35	1.2	4.8×10^5
25	25	68	27	2.5	6.8×10^5

In Fig. 3, the steady shear viscosity, η is plotted as a function of shear rate, $\dot{\gamma}$ for the three fluids used. At small shear rates the response of the fluid is Newtonian and the viscosity is constant. As the shear rate is increased, the fluids begin to shear thin very heavily; the shear stress plateaus with increasing shear rate and the viscosity dependence on shear rate approaches a slope of $\eta \propto \dot{\gamma}^{-1}$. For the sake of completeness, the important rheological parameters of each solution are presented in Table 1. A more

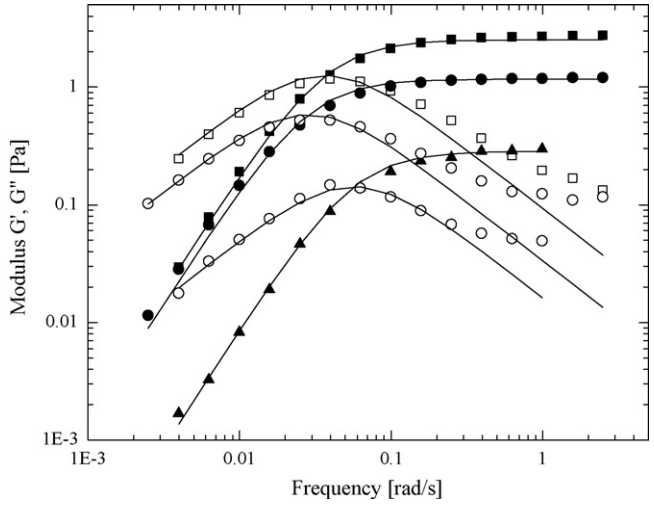

Fig. 2. Linear viscoelastic shear rheology of the wormlike micelle solutions used. The filled symbols denote the storage modulus G' while the open symbols denote the loss modulus G''. The data include aqueous solutions of: (▲) 10 mM CTAB and 10 m M NaSal; (●) 17.5 mM CTAB and 17.5 mM NaSal; (■) 25 m M CTAB and 25 mM NaSal; and (—) the fit from a single mode Maxwell model.

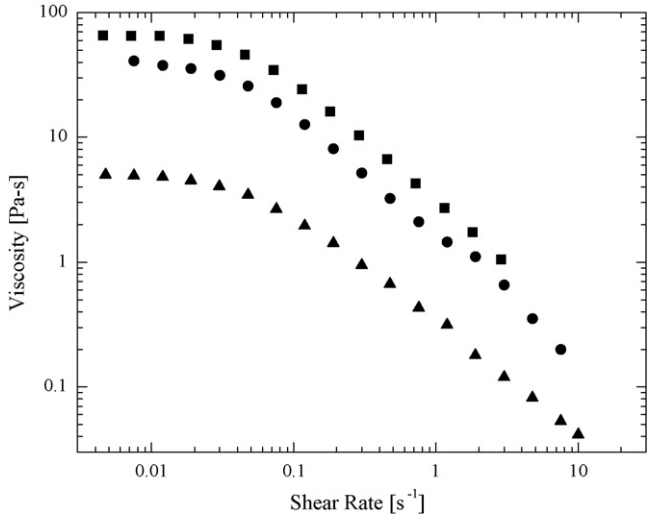

Fig. 3. Steady shear rheology of the wormlike micelle solutions used. The experimental data include aqueous solutions of: (▲) 10 mM CTAB and 10 m M NaSal; (●) 17.5 mM CTAB and 17.5 mM NaSal; (■) 25 mM CTAB and 25 mM NaSal.

complete discussion of the fluid shear rheology and the rheological models used to fit the data can be found in our recent publications [12,28]. For comparison, water with viscosity of $\mu = 0.001$ Pa s was also used in both the flat-fan and hollow-cone spray nozzles.

2.4. Extensional rheology

Strain hardening of the extensional rheology of polymer solutions and wormlike micelle solutions has been shown to stabilize viscoelastic jets while retarding satellite drop formation and increasing the main droplet size [11,13,14,20,21]. Therefore, it is important to characterize the response of the test fluids in both shear and extensional flows. Capillary break-up extensional rheometry (CaBER) measurements [19,29–33] were performed using a filament stretching rheometer [12,19,33,34] to drive the initial step strain required to produced the liquid bridge.

A plot of the apparent Trouton ratio, $\mathrm{Tr} = \eta_E/\eta_0$, for the three wormlike micelle solutions is presented in Fig. 4 as a function of Hencky strarn, $\varepsilon = -2\ln(R_{mid}/R_0)$. Here R_{mid} is the radius of the fluid filament, R_0 the initial filament radius, η_E the extensional viscosity and η_0 is the zero shear rate viscosity. The extensional viscosity of each of the fluids was found to strain harden and approached an equilibrium value at large Hencky strains. For a point of comparison, the Trouton ratio for a Newtonian fluid is independent of strain and equal to $\mathrm{Tr} = 3$. The value of the Trouton ratio was found to increase with decreasing surfactant concentration. This is consistent with the previous literature which showed that for a both entangled wormlike micelle solutions and entangled polymer solution that the degree of strain hardening decreases with increasing concentration [12,19,33,35]. However, unlike polymer solutions, wormlike micelle solutions have been found to fail in strong extensional flows imposed by filament stretching rheometers through a dramatic rupture of the fluid filament near its axial midplane [12,19,33,36]. Similar rupture events were also observed for wormlike micelle solutions in pendent drop experiments [37]. This filament failure likely stems from the scission of wormlike micelles resulting in a dramatic breakdown of the micelles *en masse* [12] and are likely to have great significance to a number of industrial flows of wormlike micelle solutions, including the atomization of spays, where strong extensional flow are often encountered.

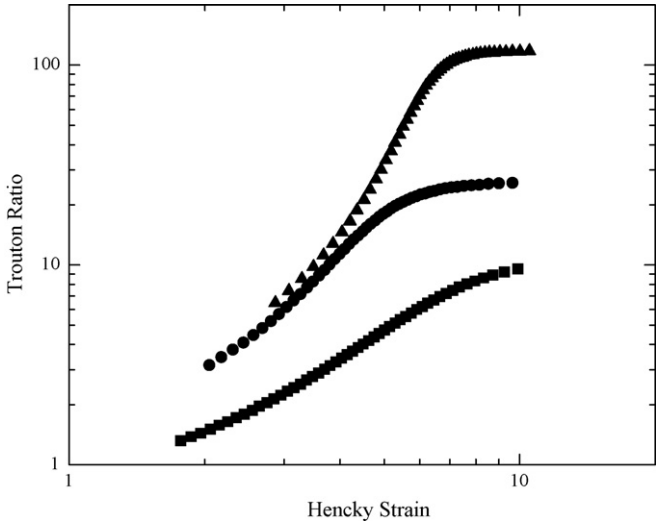

Fig. 4. Transient homogeneous uniaxial extensional rheology. The Trouton ratios were measured using a capillary break-up extensional rheometer and are all performed at a Deborah number of $De = 2/3$. The experimental data include aqueous solutions of: (▲) 10 mM CTAB and 10 m M NaSal; (●) 17.5 mM CTAB and 17.5 mM NaSal; (■) 25 mM CTAB and 25 mM NaSal.

3. Results and discussion

3.1. Flat-fan nozzles

When the thin liquid sheet produced by both the hollow-cone and flat-fan nozzles are composed of Newtonian fluids like water, the resulting fluid dynamics are controlled by a balance of inertial, gravitational and capillary stresses. At sufficiently high speed and Reynolds and Froude numbers, the effects of gravity can be neglected. When the fluid is viscoelastic, elastic stresses must also be considered, resulting in changes to both the kinematics and stability of the thin film. The spray nozzles are designed to produce a flow which is spread radially outward at an angle between $65° < \beta < 120°$. As seen in Fig. 5, surface tension and elasticity resist the spread of the thin film and ultimately restrict its size resulting in the formation of a relatively thick rim around the film in the case of the flat-fan nozzle. As we will discuss in Section 3.2 and can be seen in Fig. 16, no such rim is formed for the case of the hollow-cone nozzle. For the flat-fan nozzle, the sheet eventually closes back in upon itself forming an apex below the nozzle exit and giving the sheet a leaf-like appearance.

As seen in Fig. 5, as the volume flow rate of the fluid through the flat-fan nozzles is increased, the fluid sheet expands in size and transitions through a series of different flow regimes. Aerodynamic forces or, in some cases, a rim instability [22] are the source of the onset of the initial disturbances in the fluid sheet. Oscillations in the fluid sheet become more pronounced with increasing flow strength. For low viscosity Newtonian fluids such as water, these oscillations continue to grow with flow strength resulting in an out-of-plane flapping motion that eventually results in the atomization of the sheet [2,10]. These out-of-plane oscillations can be observed in Fig. 6. As the concentration of surfactant increases, the increased viscosity and elasticity of the fluid are observed to dampen the out-of-plane oscillations of the fluid sheet causing the subsequent break-up to move to larger flow rates.

Above a critical flow rate, the sheets produced by the flat-fan nozzles were observed to become unstable, eventually atomizing into drops. The atomization process occurs very differently for the Newtonian and viscoelastic fluids tested here. As seen in Fig. 7A, the rims of the water sheets were observed to form fingers. These fingers were then observed to grow with time or distance from the nozzle eventually breaking up into drops and destabilizing the fluid sheet from the edges in towards the center of the thin film. For the viscoelastic wormlike micelle solutions in Fig. 7B, the rim remains stable and coherent while sheet expe-

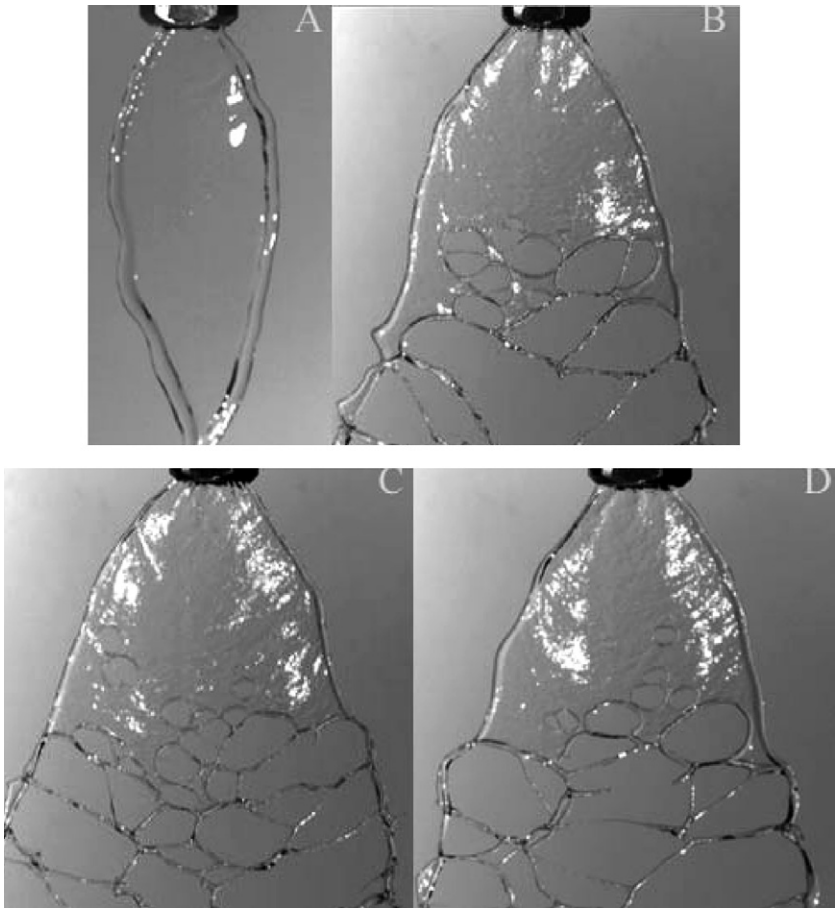

Fig. 5. The effects of flow rate increase on fluid sheet break-up are shown for Weber numbers of (A) $We = 1.2 \times 10^3$, (B) 4.9×10^3, (C) 1.1×10^4, and (D) 2.0×10^4 with 10 mM CTAB/NaSal and a 65° flat-fan nozzle.

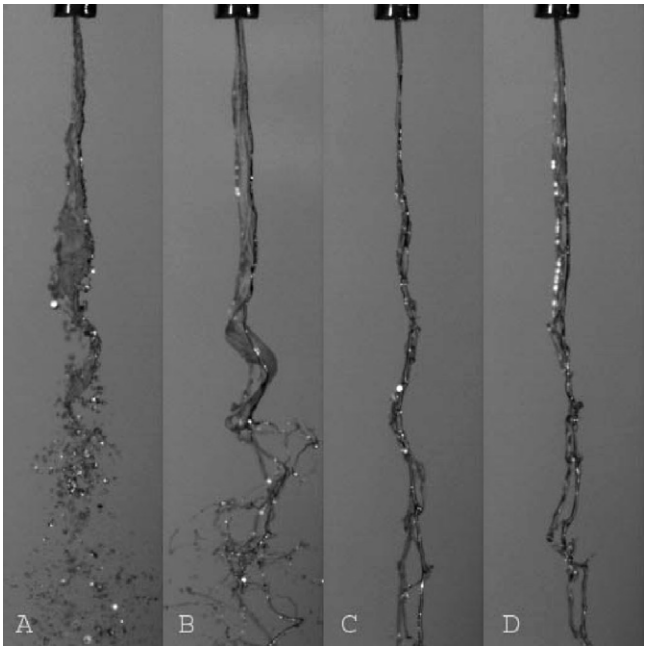

Fig. 6. Effects of aerodynamic-induced oscillations on the break-up of (A) water and (B) 10 mM (C) 17.5 mM (D) 25 mM CTAB/NaSal for a 65° nozzle and a volume flow rate of 4.8×10^{-6} m^3/s (Weber number of $We = 3.0 \times 10^3$ for (A) and $We = 4.9 \times 10^3$ for (B), (C) and (D)).

riences a number of randomly located internal failures. As the capillary and elastic stresses retract the sheet from the rapidly expanding hole, an internal rim is formed. As shown in Fig. 5, the frequency of the internal sheet rupture events increases with increasing flow rate. As the internal rims produced by multiple rupture collide to produce a complicated interconnected, a structure is formed which is similar to the 'fluid webs' observed by Miller et al. [9] which resulted from impinging two obliquely aligned jets of viscoelastic wormlike micelle solutions.

The stabilization of the sheet rims with increasing fluid elasticity is not altogether unexpected. Strain hardening of the extensional viscosity of these wormlike micelle solutions can result in a viscoelastic-capillary timescale of as much as $\tau_E = \eta_E R/\sigma \approx 6$ s while for water the break-up of the rim is governed by a Raleigh timescale of approximately $\tau_R = \sqrt{\rho R^3/\sigma} \approx 10^{-3}$ s. On the other hand, the destabilization of the internal fluid sheet with the addition of fluid elasticity is less intuitive. Our observations do, however, agree well with the linear stability theory of Brenn et al. [10] who showed that viscoelastic fluid sheets were less stable than Newtonian fluid sheets to internal failures resulting from infinitesimal out-of-plane perturbations of the fluid sheets.

In Figs. 8 and 9, the progression of the flow structures, shown in Figs. 5 and 7, are mapped out in a diagram showing the dependence of the structure on the fan angle and the governing dimensionless groups; the elasticity number which is a ratio of

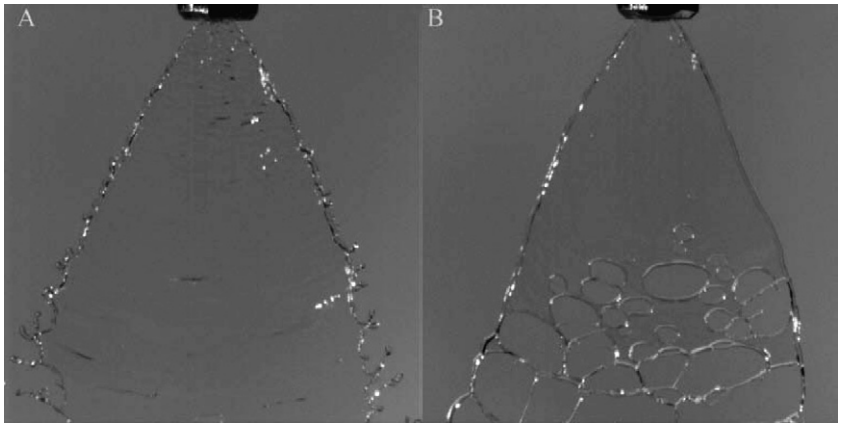

Fig. 7. The images show (A) unstable water rim and (B) stable viscoelastic rim for the 17.5 mM CTAB/Nasal solution at a volume flow rate of 4.8×10^{-6} m^3/s using a 65° flat-fan nozzle.

the Weissenberg and Reynolds numbers, $\mathrm{El} = Wi/Re = \lambda\eta_0/\rho R^2$, and the Weber number, $We = \rho U^2 D/\sigma$. Here R and D are the radius and diameter of the nozzle orifices, respectively. The elasticity numbers is a material property independent of flow rate and is given in Table 1 for each of the wormlike micelle solutions. The dimensionless groups chosen here represent a single slice in a multidimensional parameter space containing all the possible dimensionless groups. The elasticity number and Weber number were chosen to highlight the importance of elasticity, inertia and surface tension while insuring that only one axis was a function of flow rate. A side-by-side comparison between the atomization of water and the viscoelastic 17.5 mM CTAB/NaSal solution at the same flow rate in Fig. 7 clearly shows that the addition of elasticity forestalls the onset of the rim instability, but destabilizes the internal sheet. However, if one compares two viscoelastic fluids, one finds that although a small amount of viscoelasticity destabilizes the internal sheet when compared to the atomization of a Newtonian fluids, further increasing the elasticity of the fluid was found to forestall each of the identifiable flow transitions. In addition, increasing the flat-fan angle was found to destabilize the fluid sheets. The stability diagrams in Figs. 8 and 9 are for only the 65° and 120° nozzles, respectively. The results for the 30° nozzle are not shown because the sheets of all the viscoelastic wormlike micelle solutions were stable for all the experimentally obtainable flow rates. Comparing Figs. 8 and 9, it can be observed that increasing the nozzle angle destabilizes the fluid sheet and improves atomization. Take for example the 25 mM CTAB/NaSal solution, $\mathrm{El} = 8.7 \times 10^5$, for which the critical Weber number for the onset of internal sheet rupture is found to decrease by nearly 30%, from $We = 3.4 \times 10^3$ to 2.4×10^3, as the nozzle angle is increased from 65° and 120°. This is demonstrated by the images presented in Fig. 10 which clearly show an increased size and number of holes in the fluid sheet with increasing nozzle angle.

In order to analyze the high-speed video quantitatively, the images were imported into Matlab™ and a series of measure-

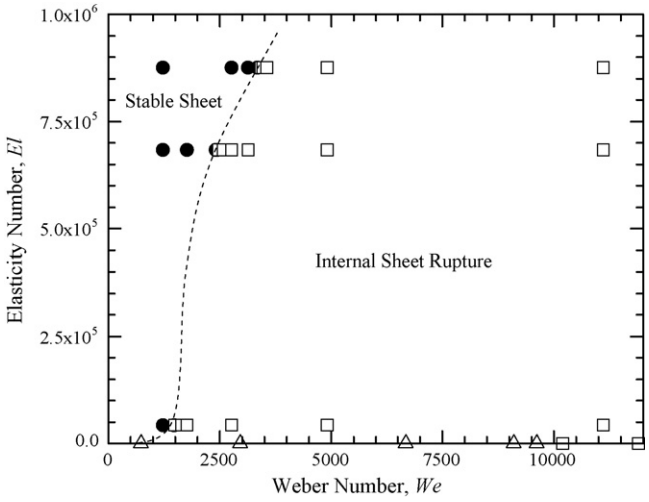

Fig. 8. Diagram illustrating the dependence of the stability and structure on flow strength and fluid rheology for the 65° flat-fan nozzle. The symbols represent: '●', a stable sheet; '△', an unstable rim; and '□', internal sheet rupture. Borders between the flow regimes are not quantitative, but are meant only to guide the reader's eye.

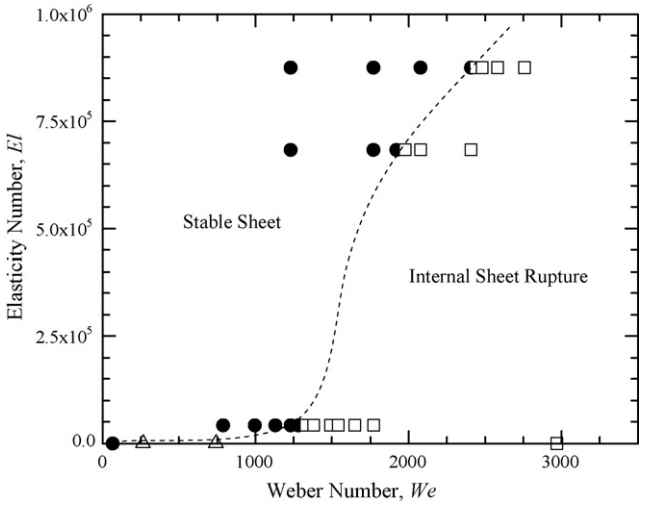

Fig. 9. Diagram illustrating the dependence of the stability and structure on flow strength and fluid rheology for the 120° flat-fan nozzle. The symbols represent: '●', a stable sheet; '△', an unstable rim; and '□', internal sheet rupture. Borders between the flow regimes are not quantitative, but are meant only to guide the reader's eye.

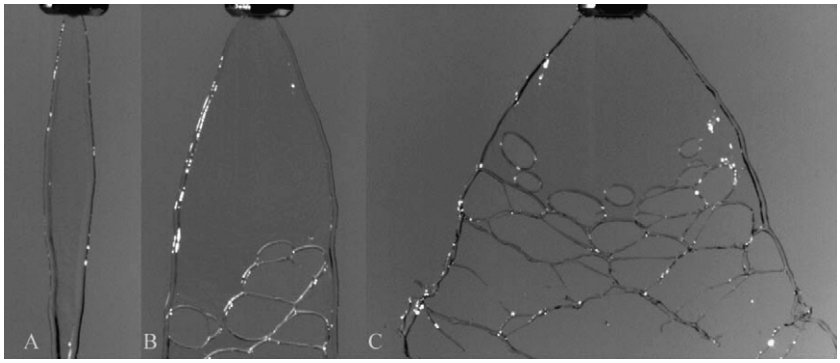

Fig. 10. Increased nozzle angle improved sheet break-up for the10 mM CTAB/NaSal solution at a Weber number of $We = 4.9 \times 10^3$ as shown by the (A) 30° (B) 65° and (C) 120° nozzles.

ments were made to further investigate the break-up dynamics of the fluid sheets. Because the large extensional viscosities of these micelle solutions tend to retard the break-up of the interconnected internal fluid rims making up the fluid webs, measurements of drop size and distribution were difficult. The fluid webs were extremely long-lived, remaining coherent for tens of centimeters downstream of the nozzle. Our measurements thus focused instead on how quantities such as the spread angle of the sheet, initiation time of sheet rupture, growth rate of the holes within the sheet, and the number and size of holes at several distances downstream of the nozzle exit changed with nozzle angle, flow rate and fluid properties. In Fig. 11, the spray angle is plotted as a function of flow rate for the 65° and 120° nozzles and the 10, 17.5 and 25 mM solutions. None of the solutions achieved the design angle of the nozzle. Increases to the flow rate had little effect on the expansion angle of the fluid sheet, but increasing elasticity was found to dramatically reduce the expansion angle of the fluid sheet. The effects of elasticity were significantly more pronounced with increasing nozzle angle and the increasing strength of the extensional flow produced within the expanding sheet.

In many applications, it is advantageous to atomize the fluid very quickly. In Fig. 12, the average time needed to initiate sheet rupture is plotted as a function of flow rate for the 65° and 120° nozzles and the 10, 17.5 and 25 mM solutions by dividing the initial rupture location by the average velocity of the flow. The sheet is observed to rupture more quickly with increasing flow rate, nozzle fan angle and fluid elasticity. One interesting observation is that the break-up time seems to become less sensitive to parameters like nozzle angle and fluid elasticity with increasing flow rate. If we had instead measured the position of the initial sheet rupture as a function of flow rate, the curve would be non-monotonic; initially decreasing with increasing flow rate, but then approaching a plateau or even increasing at large flow rates as the perturbations in the sheet move away from the nozzle more quickly.

By measuring the size and frequency of the holes in the fluid sheets, it is possible to determine the growth rate of the holes

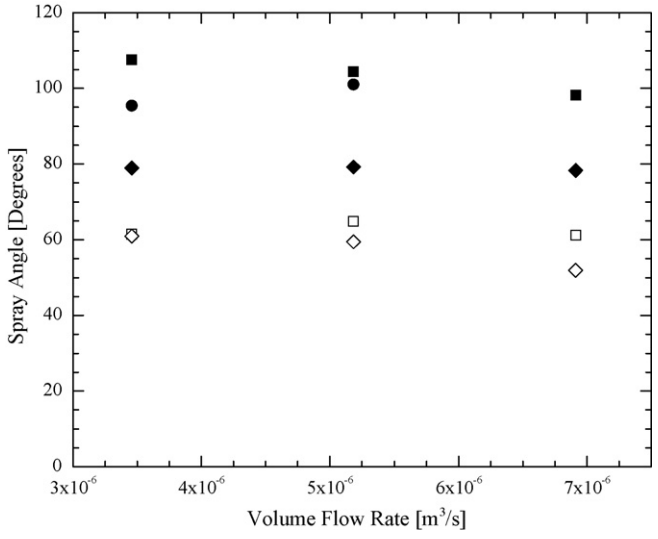

Fig. 11. The angle of the fluid sheet exiting the flat-fan nozzle as a function of volume flow rate for '■', 10 mM CTAB/NaSal solution, '●', 17.5 mM CTAB/NaSal solution, and '♦', 25 mM CTAB/NaSal solutions. The filled symbols represent a 120° flat-fan nozzle while the hollow symbols represent the 65° flat-fan nozzle.

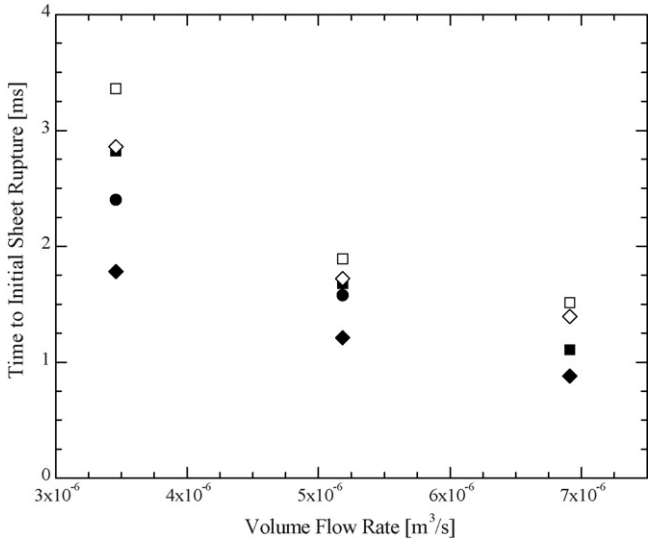

Fig. 12. The average time required for the initialization of sheet rupture as a function of volume flow rate for '■', 10 mM CTAB/NaSal solution, '●', 17.5 mM CTAB/NaSal solution, and '♦', 25 mM CTAB/NaSal solutions. The filled symbols represent a 120° flat-fan nozzle while the hollow symbols represent the 65° flat-fan nozzle.

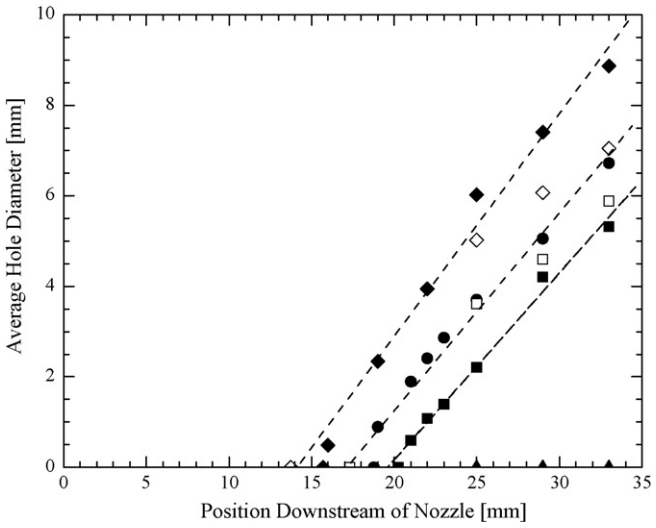

Fig. 13. The average hole diameter within the sheet formed by the flow of '▲', water, '■', 10 mM CTAB/NaSal solution, '●', 17.5 mM CTAB/NaSal solution, and '♦', 25 mM CTAB/NaSal solution through a 120° flat-fan nozzle. The solid symbols are measured at a volume flow rate of 3.5×10^{-6} m^3/s ($We = 2.8 \times 10^3$) while the hollow symbols are at 6.9×10^{-6} m^3/s ($We = 1.1 \times 10^4$). The dashed lines are a linear fit to the data.

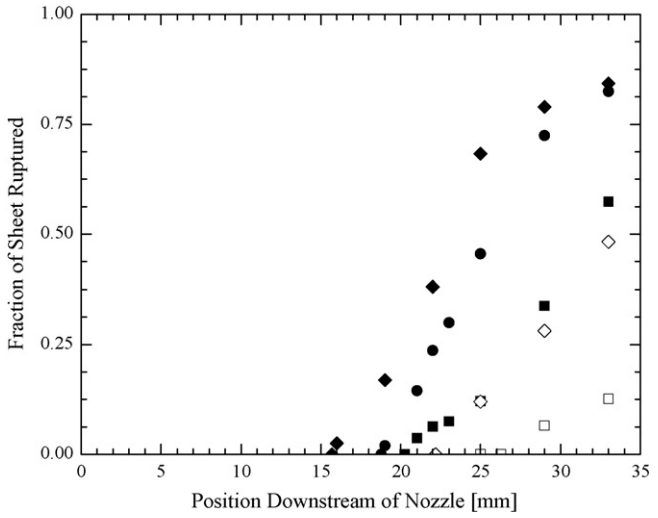

Fig. 14. The average fraction of the sheet ruptured as a function of position downstream of the nozzle for the flow of '■', 10 mM CTAB/NaSal solution, '●', 17.5 mM CTAB/NaSal solution, and '♦', 25 mM CTAB/NaSal at a volume flow rate of 3.5×10^{-6} m^3/s ($We = 2.8 \times 10^3$). The hollow symbols represent the 65° flat-fan nozzle and the filled symbols represent the 120° flat-fan nozzle.

and estimate the eventual drop size distribution. In Fig. 13, measurements of the average hole diameter were taken at several locations downstream of the nozzle exit for each of the wormlike micelle solutions and volume flow rate of 3.5×10^{-6} m^3/s ($We = 2.8 \times 10^3$) and 6.9×10^{-6} m^3/s ($We = 1.1 \times 10^4$). As observed in Fig. 12, increasing the fluid elasticity destabilizes the sheet causing it to rupture closer to the nozzle exit. As seen in Fig. 13, the initial hole growth is very fast and is likely the result of the release of the elastic potential energy built up within the sheet as the flow expands and stretches out of the nozzle. The growth rate of the holes which can be calculated as the slope of the data in Fig. 13 multiplied by the velocity of fluid. After the initial fast growth, in the sheet appears to slow and the average hole size begins to increase linearly with increasing position and time. An interesting observation is that the long time growth rate of the holes in the sheet appears to be nearly independent of fluid elasticity, increasing only very slightly with increasing surfactant concentration and elasticity. This suggests that the long time growth of the holes is governed by a balance of capillary forces and inertia because each of the solutions has similar surface tension and density it would follow that the velocity of a hole growth governed by these parameters would be independent of the surfactant concentration and rheological properties. However, calculations of an inertio-capillary or Rayleigh velocity defined as $u_R = (\sigma/R\rho)^{1/2} \approx 0.5$ m/s results in a velocity which is an order of magnitude larger than the observed growth rate of the holes within the sheet is approximately $u_h \approx 1$ mm/s. Additionally, the growth rate of the holes is an order magnitude smaller than both the elastic wave speed, $u_{el} = \sqrt{G/\rho}$, and the capillary velocity, $u_{cap} = \sigma/\eta_0$, both of which are order 10 mm/s and additionally are strong functions of fluid rheology. If, however, we calculate a viscoelastic-capillary velocity using the extensional and not the shear viscosity, the resulting velocity is of the correct order, $u_{ve} = \sigma/\eta_E \approx 0.5$ mm/s, and the result is nearly independent of surfactant concentration. This can be understood by inspecting the equilibrium Trouton ratios of the three fluids in Fig. 4. The Trouton ratio is found to increases with decreasing surfactant concentration and at the same time the shear viscosity is found to decrease with decreasing surfactant concentration. The end result of these two trends is an equilibrium extensional viscosity which is not very sensitive to the surfactant concentration. This suggests that after the initial formation of the holes, their expansion is governed by a balance of the capillary stresses and the extensional stresses developed within the flow.

To further determine the degree of atomization, the average fraction of the sheet ruptured is plotted as a function of position downstream of the nozzle in Fig. 14. The fraction of the sheet ruptured is calculated by dividing, for a given cross-section of the sheet, the total length of holes bisected by the width of the sheet. The fraction of sheet ruptured initially grows linear with position (or time), but as the holes begin to interact on the sheet, an internal rim structure is formed and the degree of sheet rupture asymptotes at a value between 80% and 90% of the sheet. The dynamics of hole growth and interaction are shown in Fig. 15 which shows a time series of hole growth for each of the three wormlike micelle solutions. The time between images is 1/4000th of a second and the images clearly show the speed at which the holes grow and the way they interact to form a web-like structure. The eventual size of the atomized droplets can be estimated by measuring the diameter of the interconnected fluid filaments; the final fluid drop sizes will increase with increasing filament size. From Fig. 15, it is clear that increases in fluid elasticity results in an increase in the thickness of the interconnecting fibrils of the fluid webs. One therefore expects to observe an increase in the average final drop size with increasing fluid elasticity even though the fluid sheet tends to rupture more quickly and more often with increasing fluid elasticity.

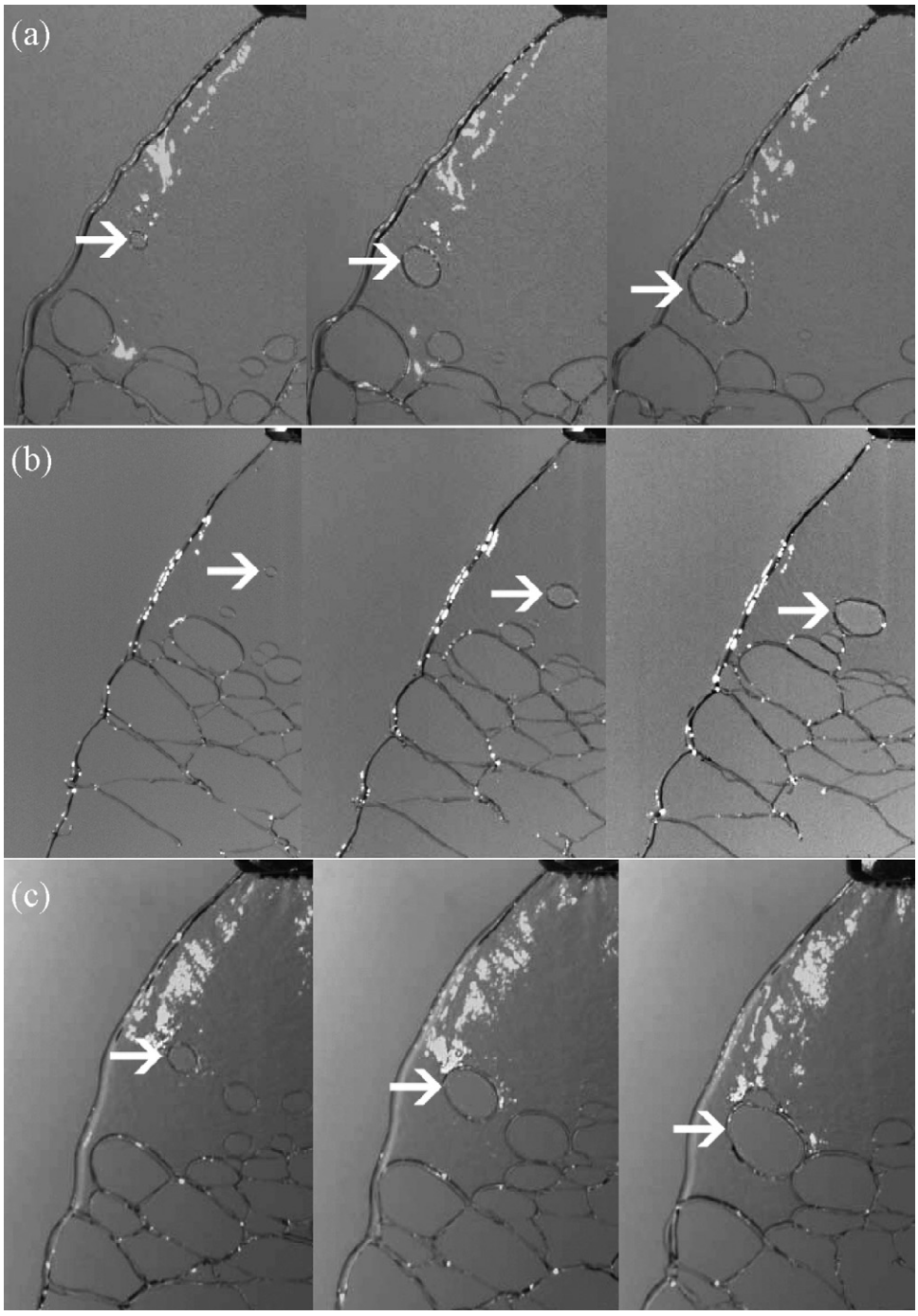

Fig. 15. Time series of images showing the evolution and growth of holes in sheets of (a) 10 mM CTAB/NaSal, (b) 17.5 mM CTAB/NaSal and (c) 25 mM CTAB/NaSal produced by a 120° flat-fan nozzle at Weber number of $We = 2.8 \times 10^3$.

3.2. Hollow-cone nozzles

Swirl-type hollow-cone nozzles rely on fluid inertia to throw the fluid to the outside of the nozzle, overcome surface tension and produce a hollow cone. For low viscosity fluids such as water this design has been found to work very well, however, for higher viscosity fluids such as the wormlike micelle solutions tested here, the Reynolds number can be quite small ($0.01 < Re < 10$) and viscous effects can dominate over inertial effects. However, as the flow rate and subsequently the shear rate within the tubing upstream of the nozzle and nozzle itself is increased, the shear viscosity of the wormlike micelle solutions will shear thin to values very close to that of water as seen in Fig. 3. The transitions from jetting to complete atomization of the hollow cone are shown in Fig. 16 for the 10 mM CTAB/NaSal wormlike micelle solution for a series of increasing flow rates. Many of the flow transitions observed in Fig. 16 are observed for both water and the viscoelastic wormlike micelle solutions, however, the previously unobserved flow phenomena seen in Fig. 16c and d are clearly a direct result of the fluid elasticity.

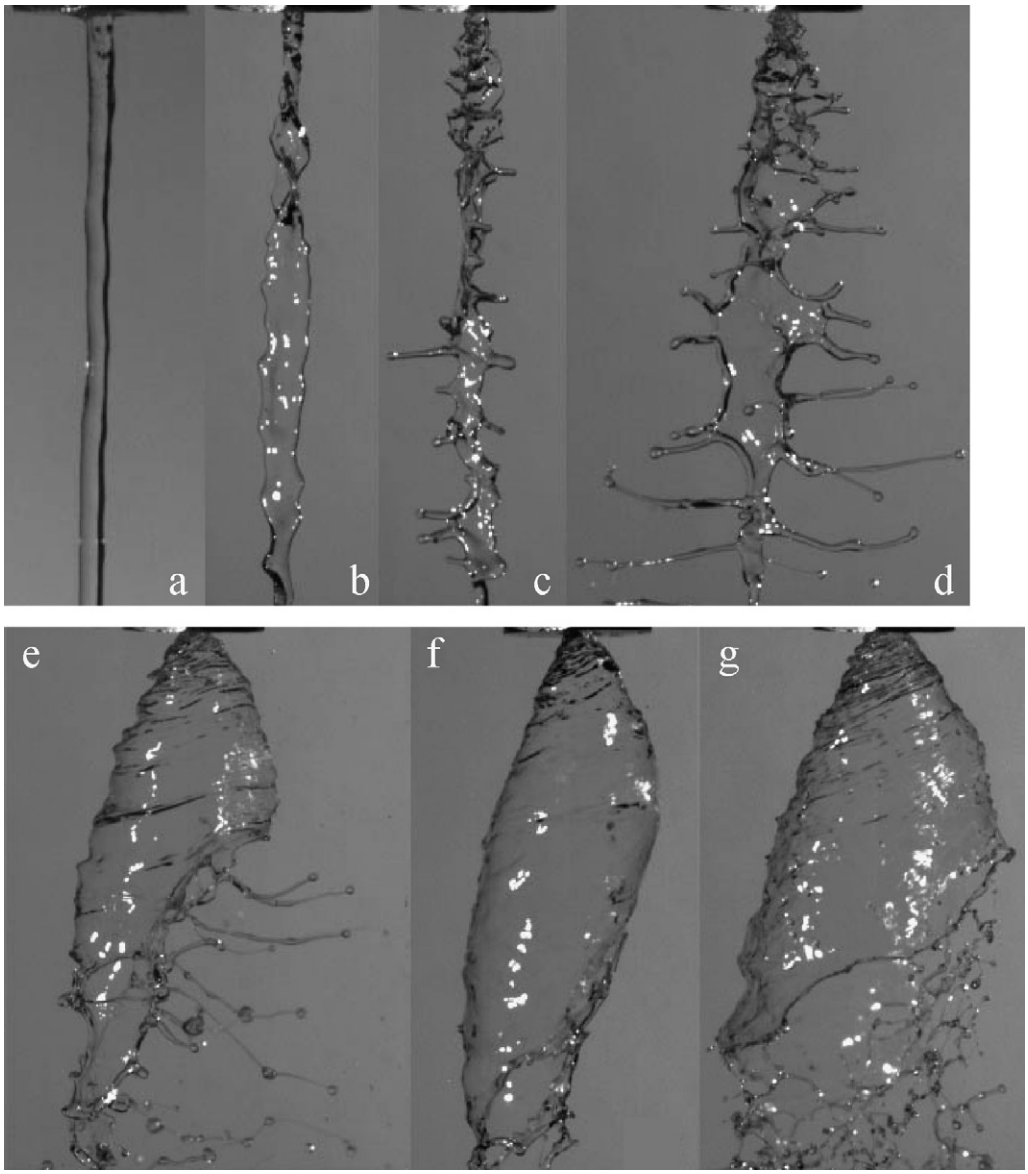

Fig. 16. The effects of flow rate increase on fluid sheet break-up are shown for 10 mM CTAB/NaSal for volume flow rates of (a) 1.9×10^{-6} m^3/s ($We = 8.2 \times 10^2$), (b) 2.4×10^{-6} m^3/s ($We = 1.3 \times 10^3$), (c) 2.7×10^{-6} m^3/s ($We = 1.7 \times 10^3$), (d) 2.8×10^{-6} m^3/s ($We = 1.8 \times 10^3$), (e) 2.9×10^{-6} m^3/s ($We = 1.9 \times 10^3$), (f) 3.1×10^{-6} m^3/s ($We = 2.2 \times 10^3$), and (g) 3.6×10^{-6} m^3/s ($We = 2.9 \times 10^3$) from a hollow-cone nozzle.

At low flow rates, a rotating fluid jet is produced from the hollow-cone nozzle; see Fig. 16a. As the flow rate and subsequently the rotation rate of the jet are increased, the jet transitions from a circular cross-section to a much flatter cross-section taking on a twisted ribbon-like appearance; see Fig. 16b. As the rotation rate is increased further, the edges of the ribbon are destabilized, fingers grow and are ejected outward by the fluid inertia; see Fig. 16c. The length of the fingers grow with increasing flow rate and because of the large extensional viscosity of the wormlike micelle solutions, they remain remarkably coherent forming intricate structures resembling 'fluid trees'; see Fig. 16d. Close inspection of the 'fluid trees' near the nozzle exit in Fig. 16d shows the early formation of the hollow-cone. With further increase in the flow rate the fluid trees gradually transition into a partial cone; see Fig. 16e. This partial cone eventually closes in upon itself forming a stable, closed hollow cone; see Fig. 16f. The stable closed cone is observed only for water and the lowest concentration wormlike micelle solution. Additionally, the stable closed cone was observed over a very small range of flow rates, eventually becoming unstable and atomizing with increasing flow rate; see Fig. 16g.

The progression of the flow structures shown in Fig. 16, are mapped out in Fig. 17 in order to illustrate the dependence of the structure on the governing dimensionless groups; the elasticity number and the Weber number. The figures clearly show that the addition and increase of elasticity forestalls all of the identifiable flow transitions and the eventual atomization of the fluid sheets. For a given Weber number, increasing elasticity was found to increase the distance from the nozzle that atomization was initiated, generally reduce the quality and degree of atomization, while reducing both the angle and width of the resulting cone. Whereas elasticity was found to destabilize the fluid sheet in

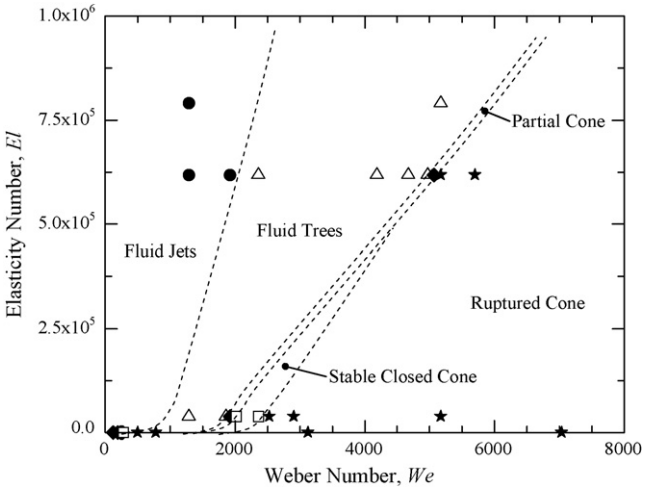

Fig. 17. Diagram illustrating the dependence of the stability and structure on flow strength and fluid rheology for the hollow-cone nozzle. The symbols represent: '●', fluid jets; '▲', fluid trees; '♦', partial cone; '□', stable closed cone; and '★', ruptured cone. Borders between the flow regimes are not quantitative, but are meant only to guide the reader's eye.

flat-fan nozzles, it clearly stabilizes the sheet formed by hollow-cone spray nozzles.

4. Conclusions

A series of experiments were performed to investigate the flow kinematics and stability of thin viscoelastic fluid sheets produced by a series of commercially available flat-fan and hollow-cone spray nozzles. The viscoelastic wormlike micelle solutions used in these experiments were produced by mixing a surfactant, CTAB, and salt, NaSal, in water at a series of different concentrations to vary the viscoelasticity of the fluids. As the flow rate through the nozzles was increased, the viscoelastic fluid sheets were found to grow larger; eventually become unstable, and atomizing into drops. For the flat-fan spray-nozzles, Newtonian water sheets were found to first destabilize along the fluid rim. The addition of viscoelasticity was found to stabilize the rim while simultaneously destabilizing the fluid sheet. The internal rims produced by multiple rupture eventually collide within the fluid sheet to produce a complicated highly interconnected structure which is similar to the 'fluid webs' observed by Miller et al. [9]. Increasing the viscoelasticity of the test fluid was found to stabilize the thin films produced by both the flat-fan and hollow-cone spray nozzles. However, even though viscoelasticity was found to forestall the break-up of these fluid sheets to larger flow rates once the flow rate was increased beyond the critical flow rate for sheet rupture, increasing the fluid elasticity was found to enhance the atomization of the viscoelastic fluid sheets by increasing the number and growth rate of holes in the sheet while simultaneously reducing the initiation time for sheet rupture. Although drop size distribution measurements were not possible in these experiments, based on the increasing size of the interconnecting fluid filaments within the ruptured sheet one would expect an increase in the final atomized drop size with increasing elasticity.

References

[1] C.J. Clark, N. Dombrowski, Aerodynamic instability and disintegration of liquid sheets, Proc. Roy. Soc. Lond. A 329 (1972) 467–478.
[2] N. Dombrowski, R.P. Fraser, A photographic investigation into the disintegration of liquid sheets, Phil. Trans. Roy. Soc. Lond. A 247 (1954) 101–130.
[3] Y.-J. Choo, B.-S. Kang, The velocity distribution of the liquid sheet formed by two low-speed impinging jets, Phys. Fluids 14 (2002) 622–627.
[4] G.I. Taylor, The dynamics of thin sheets of fluids. III. Disintegration of fluid sheets, Proc. Roy. Soc. Lond. A 253 (1959) 313–321.
[5] L.-L. Xing, J.E. Glass, Parameters influencing the spray behavior of waterborne coatings, J. Coatings Technol. 71 (1999) 3750.
[6] R.P. Mun, B.W. Young, D.V. Boger, Atomization of dilute polymer solutions in agricultural spray nozzles, J. Non-Newton. Fluid Mech. 83 (1999) 163–178.
[7] M. Stelter, G. Brenn, F. Durst, The influence of viscoelastic fluid properties on spray formation from flat-fan and pressure-swirl atomizers, Atomization Sprays 12 (2002) 299–327.
[8] G.M. Harrison, R.P. Mun, G. Cooper, D.V. Boger, A note on the effect of polymer rigidity and concentration on spay atomization, J. Non-Newton. Fluid Mech. 85 (1999) 93–104.
[9] E. Miller, E. McWilliams, B. Gibson, J.P. Rothstein, The collision of viscoelastic jets and the formation of fluid webs, Appl. Phys. Lett. 87 (2005) 014101.
[10] G. Brenn, Z. Liu, F. Durst, Three-dimensional temporal instability of non-Newtonian liquid sheets, Atomization Sprays 11 (2001) 49–84.
[11] R.P. Mun, J.A. Byars, D.V. Boger, The effect of polymer concentration and molecular weight on the breakup of laminar capillary jets, J. Non-Newton. Fluid Mech. 74 (1998) 285–297.
[12] J.P. Rothstein, Transient extensional rheology of wormlike micelle solutions, J. Rheol. 47 (2003) 1227–1247.
[13] H.A. Stone, Dynamics of drop deformation and breakup in viscoelastic fluids, Annu. Rev. Fluid Mech. 26 (1994) 65–102.
[14] M. Renardy, A numerical study of the asymptotic evolution and breakup of Newtonian and viscoelastic jets, J. Non-Newton. Fluid Mech. 59 (1995) 267–282.
[15] L. Rayleigh, On the capillary phenomena of jets, Proc. Roy. Soc. Lond. 29 (1879) 71–97.
[16] M.A. Fontelos, J. Li, On the evolution and rupture of filaments in Giesekus and FENE models, J. Non-Newton. Fluid Mech. 118 (2004) 1–16.
[17] G.H. McKinley, Visco-elasto-capillary thinning and break-up of complex fluids, in: D.M. Binding, K. Walters (Eds.), Annual Rheology Reviews, The British Society of Rheology, Aberystwyth, Wales, UK, 2005.
[18] G.H. McKinley, T. Sridhar, Filament stretching rheometry, Annu. Rev. Fluid Mech. 34 (2002) 375–415.
[19] A. Bhardwaj, E. Miller, J.P. Rothstein, Filament stretching and capillary breakup extensional rheometry measurements of viscoelastic wormlike micelle solutions, J. Rheol., in press.
[20] M.C. Sostarecz, A. Belmonte, Beads-on-string phenomena in wormlike micellar fluids Phys, Fluids 16 (2004) L67–L70.
[21] B. Yesilata, C. Clasen, G.H. McKinley, Nonlinear shear and extensional flow dynamics of wormlike surfactant solutions, J. Non-Newton. Fluid Mech. 133 (2006) 73–90.
[22] J.W.M. Bush, A.E. Hasha, On the collision of laminar jets: fluid chains and fishbones, J. Fluid Mech. 511 (2004) 285–310.
[23] J.N. Israelachvili, Intermolecular and Surface Forces: With Applications to Colloidal and Biological Systems, Academic Press, London, 1985.
[24] H. Rehage, H. Hoffmann, Viscoelastic surfactant solutions: model systems for rheological research, Mol. Phys. 74 (1991) 933–973.
[25] P. Fischer, H. Rehage, Rheological master curves of viscoelastic surfactant solutions by varying the solvent viscosity and temperature, Langmuir 13 (1997) 7012–7020.
[26] J.-F. Berret, J. Appell, G. Porte, Linear rheology of entangled wormlike micelles, Langmuir 9 (1993) 2851–2854.
[27] A. Khatory, F. Lequeux, F. Kern, S.J. Candau, Linear and nonlinear viscoelasticity of semidilute solutions of wormlike micelles at high salt concentration, Langmuir 9 (1993) 1456–1464.

[28] J. Lampe, R. DiLalla, J. Grimaldi, J.P. Rothstein, The impact dynamics of droplets on thin films of viscoelastic wormlike micelle solutions, J. Non-Newton. Fluid Mech. 125 (2005) 11–23.
[29] L.E. Rodd, T.P. Scott, J.J. Cooper-White, G.H. McKinley, Capillary break-up rheometry of low-viscosity elastic fluids, Appl. Rheol. 15 (2005) 12–27.
[30] S.L. Anna, G.H. McKinley, Elasto-capillary thinning and breakup of model elastic liquids, J. Rheol. 45 (2001) 115–138.
[31] G.H. McKinley, A. Tripathi, How to extract the Newtonian viscosity from capillary breakup measurements in a filament rheometer, J. Rheol. 44 (2000) 653–670.
[32] M. Stelter, G. Brenn, A.L. Yarin, R.P. Singh, F. Durst, Validation and application of a novel elongational device for polymer solutions, J. Rheol. 44 (2000) 595–616.
[33] A. Bhardwaj, D. Richter, M. Chellamuthu, J.P. Rothstein, The effect of preshear on the extensional rheology of wormlike micelle solutions, Rheol. Acta, in press.
[34] J.P. Rothstein, G.H. McKinley, Inhomogeneous transient uniaxial extensional rheometry, J. Rheol. 46 (2002) 1419–1443.
[35] J.P. Rothstein, G.H. McKinley, A comparison of the stress and birefringence growth of dilute, semi-dilute and concentrated polymer solutions in uniaxial extensional flows, J. Non-Newton. Fluid Mech. 108 (2002) 275–290.
[36] S. Chen, J.P. Rothstein, Flow of a wormlike micelle solution past a falling sphere, J. Non-Newton. Fluid Mech. 116 (2004) 205–234.
[37] L.B. Smolka, A. Belmonte, Drop pinch-off and filament dynamics of wormlike micellar fluids, J. Non-Newton. Fluid Mech. 115 (2003) 1–25.